INTERACTIONS BETWEEN PLATE-BOUNDARY FORCES AND EVOLVING RESISTANCE AT MID-OCEAN RIDGES AS THE ORIGIN OF NON-UNIFORM SEAFLOOR GROWTH

by

Hee Choi

A Thesis

Submitted in Partial Fulfillment of the

Requirements for the Degree of

Master of Science

Major: Earth Sciences

The University of Memphis

April 2019

ACKNOWLEDGEMENTS

Acknowledments

ABSTRACT

Geng: [Abstract shortened according to University of Memphis Thesis Style Guide.] Abstract will be here.

TABLE OF CONTENTS

LIST OF FIGURES

Figures **Pages**

Chapter 1

Introduction

Mid-ocean ridge systems have been extensively studied because of their unique geological and geophysical characteristics as well as their importance in global plate tectonics. Being the longest mountain belt on the Earth, mid-ocean ridges have a total length of 80,000 km and cover over 23 percent of the Earth's surface (Peltier, 1989). Stripe patterns of magnetic anomalies parallel to the mid-ocean ridge are critical evidence for seafloor spreading and the birth of plate tectonics (Hess, 1964).

The mid-ocean ridge is the place where new oceanic crust and lithosphere are generated by partial melting of the upper mantle (Cann, 1968). Magma rising from the upper mantle extrudes onto the ocean floor and bonds to the edges of separating plates (Chen, 1992). The oceanic plates start thin and thicken by the underplating of new lithosphere from the upper mantle and the accumulation of overlying sediment layers. As it moves away from the ridge, the lithosphere is getting cooler and denser.

Numerical models for mid-ocean ridges have improved our understanding about the mid-ocean ridge system. Chen & Morgan (1990) modeled and explained mid-ocean ridge axial topography by adopting power-law rheology. Buck & Poliakov (1998) developed a simple way to parameterize the complex process of magmatic accretion at a spreading center. Buck et al. (2005) and Tucholke et al. (2008) showed that differences in magmatic input to dikes produce the different modes of faulting at mid-ocean ridges. Behn & Ito (2008) suggested that a number of factors such as lithospheric structure and rheology controls fault growth, although the dominant factor is the ratio of magmatic accretion to the rate far field extension.

These previous studies have assumed the accretion of oceanic lithosphere at spreading centers to occur symmetrically and at a constant rate, but this assumption is not consistent with various observations (Castelino et al., 2016; Flament et al., 2014; Martinez et al., 2006; Müller et al., 1998, 2008; Fedotova et al., 2017). Castelino et al. (2016) explained anomalous bathymetry of the Mozambique basin and Riiser Larsen sea with the presence of thicker-than-usual oceanic

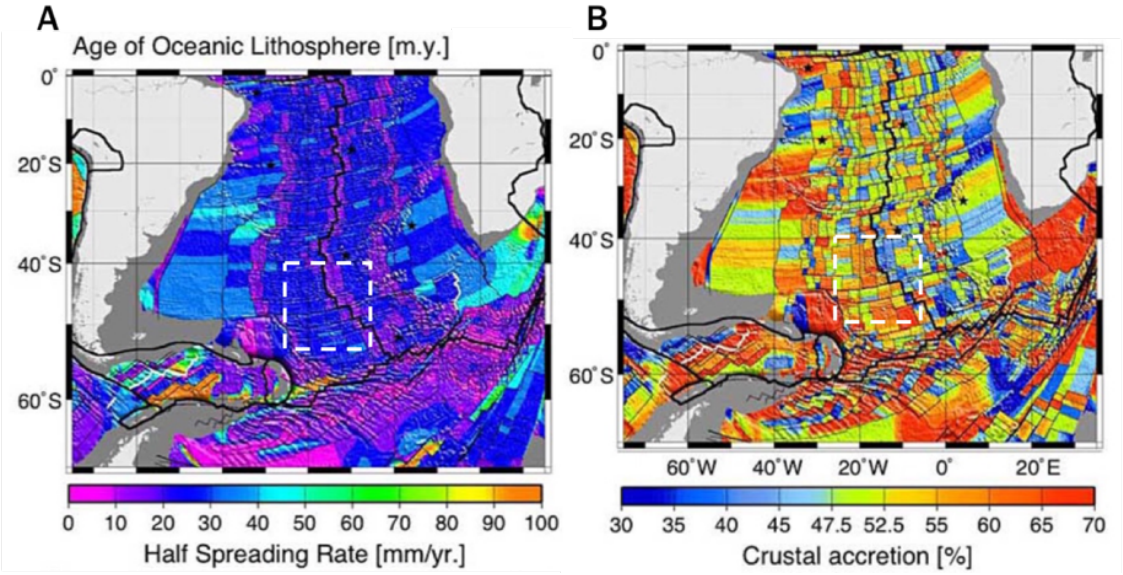

Fig. 1.1: **A.** Seafloor half-spreading rates. **B.** Crustal accretion asymmetries in the South Atlantic, Scotia Sea, and northern Weddell Sea. Dashed boxes in A and B mark the region clearly showing asymmetric features. Modified from Müller et al. (2008)

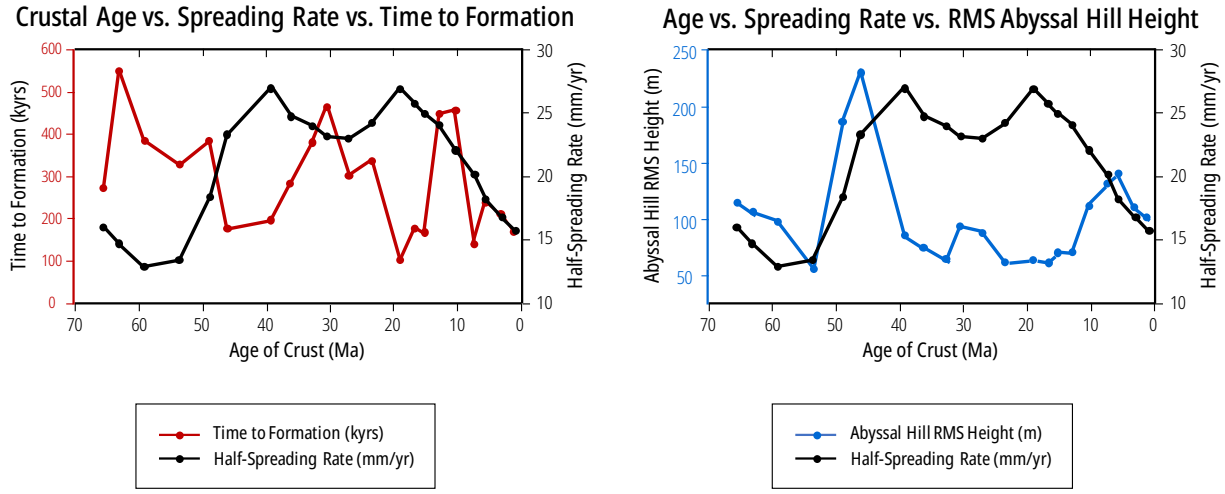

Fig. 1.2: Non-uniform half-spreading rate, crustal age, abyssal height and time to form abyssal hill data from CREST expedition in mid-Atlantinc Ridge. Digitized from Fedotova et al. (2017)

crust older than 100 Ma. Flament et al. (2014) suggested that viscous lower mantle flow may represent topographic asymmetry of the South Atlantic. Martinez et al. (2006) identified non-corresponding trends in crustal thickness and spreading rate along the back-arc Eastern Lau Spreading Center. Müller et al. (2008) set the new set of digital grids computing global depth anomalies, showed age, spreading rates, and spreading asymmetry of the world's ocean crust

(Figure 1.1). Fedotova et al. (2017) observed the half-spreading rate varies on time from CREST expedition (Figure 1.2). The asymmetric and non-uniform plate growth is not only a specific regional observation, it is a worldwide feature.

Continental rifts, another type of divergent plate boundary, has recently been shown to occur slowly during the incipient stage and accelerate later (Brune et al., 2016). Based on kinematic modeling based on plate motion inversion data from the major passive margins North Atlantic, North America – Greenland, Australia – Antarctica, and the South China sea, Brune et al. (2016) identified several rapid changes in absolute plate motion from the extension records in the major passive margins around the world, which have not been explained previously. They explained the multi-phase rifting as a result of the interaction between the evolving strength of a rift zone and forces pulling the plates apart.

Prompted by the non-uniform plate growth at mid-ocean ridges and potential interactions between the far-field forces and mid-ocean ridge processes, I investigate the mechanism of interactions between plate driving forces and internal forces at mid-ocean ridges including diking and faulting. Conventional kinematic boundary conditions are replaced with tractions in numerical models for mid-ocean ridges. I also include magmatic intrusion and faulting at a spreading center in models because magmatism and faulting play a vital role in determining characteristics of mid-ocean ridges.

Chapter 2

Methods

Magmatism at the spreading center of mid-ocean ridges plays an essential role in determining faulting styles that in turn control the axial and seafloor morphology. At fast-spreading ridges, copious magma rises and forms axial high (Figure 2.1A). With abundant magma, diking can occur frequently accommodating a significant portion of plate separation. For this reason, faults forming near axial highs have only small (i.e., 100s m) offsets (Figure 2.1A). Density variations are significant across fast-spreading ridges since the axial lithosphere is very thin, hot, and underlain by partially molten crust. Axial highs might originate from fluid magma rising to the level of local isostatic equilibrium at the plate spreading axis and then subsiding as it cools down. In contrast, faults forming at slow-spreading centers show greater offset, and axial valleys form at the spreading center (Figure 2.1B). Less abundant magma compared to fast-spreading ridges means less frequent diking and tectonic stretching accommodates a significant portion of plate separation. Faults at slow-spreading ridges develop offset up to 1-2 km. Abyssal hills produced at slow-spreading ridges are composed of faults dipping towards the axis while about half of the faults near fast-spreading centers dip toward the axis and the other half dip away from ridge axis.

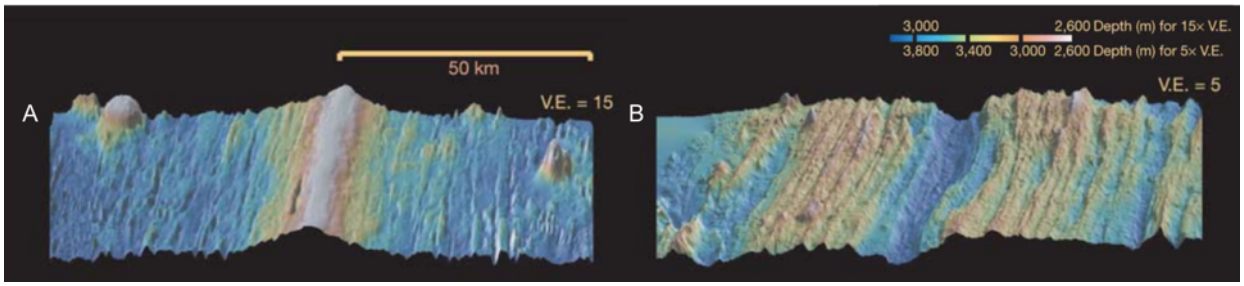

Fig. 2.1: Shaded relief images of bathymetry at slow and fast ridges. **A.** The East Pacific Rise along 9°37′N latitude **B.** The Southeast Indian Ridge along the 115°E segment. Modified from Buck et al. (2005).

Buck & Poliakov (1998) developed a simple way to parameterize the complex process of magmatic accretion at a spreading center and used it to explain the contrasting faulting styles at slow- and fast-spreading ridges. In the Buck et al. (2005) 's model, dike openings in the

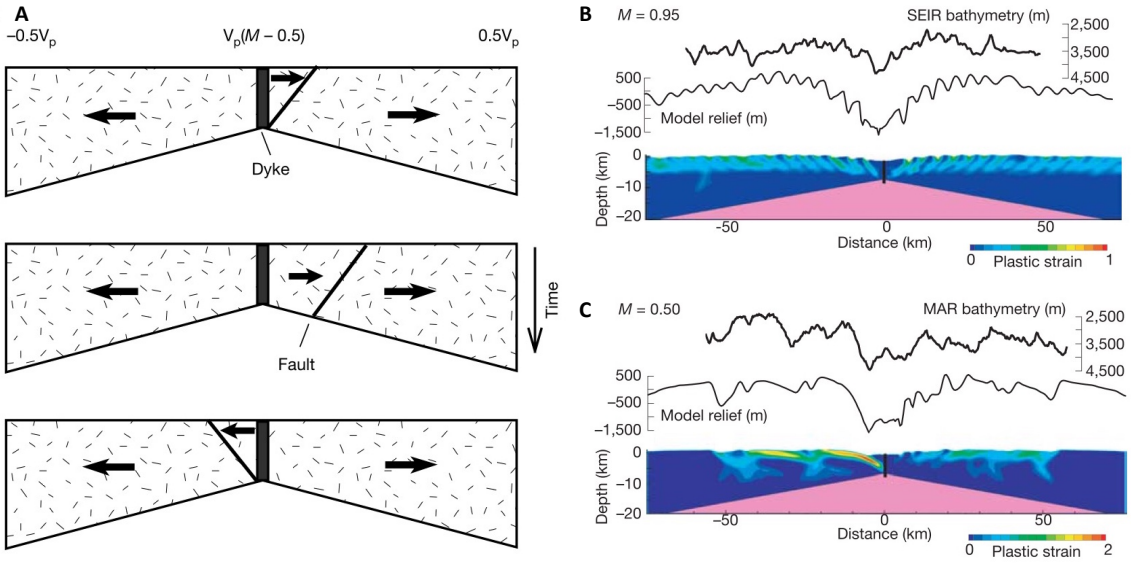

Fig. 2.2: **A.** Cartoon showing how the hanging-wall block of a fault may migrate during ridge stretching as a function of time for $0.5 < M < 1.0$. **B.** Plastic strain distribution and surface relief from the numerical model with M = 0.95. High plastic strain represents shearing on faults and the bathymetric profile across the Southeast Indian Ridge (SEIR) is shown for comparison. **C.** Same as **B** but for M = 0.5. A bathymetric profile from the Mid-Atlantic Ridge (MAR) is shown for comparison. From Buck et al. (2005)

lithosphere are taken to be uniform with depth and quantified by the ratio of dike opening rate to total plate spreading rate. This ratio is denoted as M and typically given as a parameter for a model so that the rate of diking-accommodated plate separation is determined as M times total spreading rate. When M = 0, dikes account for none of the plate spreading; and dikes accommodate all the plate separations when M = 1. M less than one corresponds to the case where magma supply is insufficient for filling the entire opening created by plate separation and tectonic stretching of the lithosphere should occurs. For M = 1, axial lithospheric separation is all taken up by dike widening and no faults and no axial valley develop. For $0.5 < M < 1$, faults develop and slip at a horizontal rate of $(1-M)$ Vp (Figure 2.2A). Since the opening by diking is faster than the rate that the fault offset increases, the fault itself is pushed off axis with time. When pushed far away from the axis, the fault locks because the lithosphere around the fault

becomes thicker and stronger. As a result, a new fault forms at the spreading center, continuing to accommodate a part of plate separation. For M = 0, dikes account for none of the plate spreading. Results for stretching-dominated ridge models are illustrated in Figure 2.2B and C. In the case of M = $\sim$1, the model produces a symmetric pattern of small-offset faults, producing a bathymetric profile similar to that of the Southeast Indian Ridge (Figure 2.2B). For M = 0.5, the model generates two large offset faults on one side, and a series of small faults on the other side. Lithospheric stretching creates conjugate normal faults at the spreading center initially. Only one branch survives on one side of the ridge, eventually evolving into a detachment fault, while short-lived new faults semi-regularly form on the opposite side. The resultant bathymetric profile resembles that of the slow-spreading Mid-Atlantic Ridge (Figure 2.2C).

Numerical approach and model setup

The FLAC (Fast Lagrangian Analysis of Continua) method (Cundall, 1982; Poliakov et al., 1993) solves the equations describing conservation of momentum

$$\frac{Dv_i}{Dt} = \frac{\partial \sigma_{ij}}{\partial x_j} + \rho g \tag{2.1}$$

and energy

$$\rho\left[\frac{\partial u_i}{\partial t} + u_j \frac{\partial u_i}{\partial x_j}\right] = -\frac{\partial P}{\partial x_i} + \rho g + \mu \frac{\partial^2 u_i}{\partial x_j \partial x_j} \tag{2.2}$$

for a visco-elastic-plastic continuum in 2-D Cartesian geometry (Lavier & Buck, 2002). By solving the conservation of momentum, the accelerations are integrated in time to give updated velocities, strains and strain rates. In addition, using the constitutive laws the strains and strain rates are used to calculate new elastic and viscous stresses. These stresses are used to determine the accelerations for the next step of calculation.

For visco-elastic deformation, the material behaves as a Maxwell solid. I follow the dry diabase power law rheology (Kirby & Kronenberg, 1987; Chen & Morgan, 1990). Plastic yielding is controlled by Mohr-coulomb theory, in which cohesion is a function of the total

accumulated plastic strain (Poliakov & Buck, 1998). Cohesion decreases linearly from its initial value 44 MPa to the minimum value of 4 MPa.

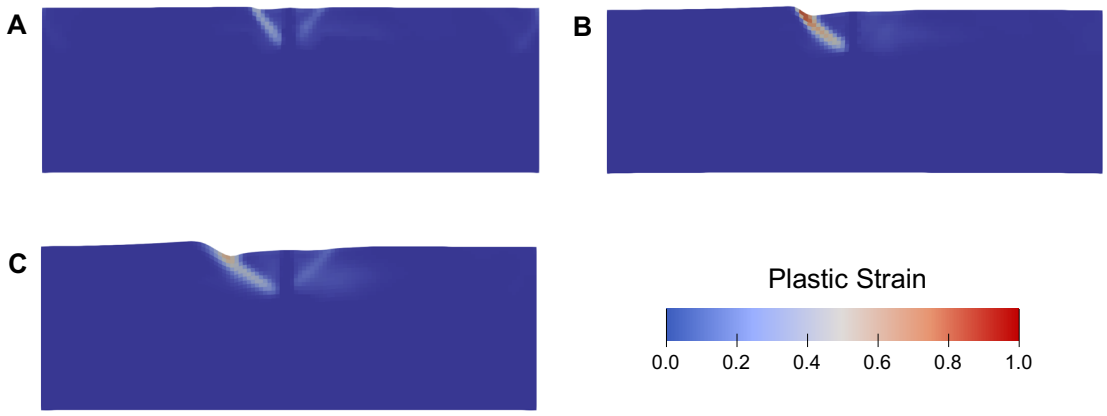

Fig. 2.3: Snapshots of the kinematic model (M = 0.8) representing stages of the fault evolution. The fault evolution can be divided as three stages. **A.** Incipient stage: new fault occurs on left side of the ridge axis. **B.** Mature stage: fault heave increases and fault dip decreases as fault grows. **C.** Terminal stage: fault becomes inactive and is replaced by a new-near axis fault on the other side of ridge axis.

The model domain is rectangular with centered ridge axis. All models have 60 km wide and 20 km deep of domain sizes with the grid of 0.5 $\times$ 0.5 km. At the top boundary, I apply seawater hydrostatic pressure while at the bottom side isostatic equilibrium is realized by means of the Winkler foundation. I apply dynamic force boundary conditions at the lateral model sides, such that at the initial stage, the boundary force is linearly increasing, allowing the plate to reach the typical sea-floor spreading rates (2.5 cm/yr). This approach is feasible if the model shows brittle failure with constant boundary forces. Hereafter, boundary force for force boundary conditioned model is defined by averaging internal force of kinematic model from the mature stage of the fault (Figure 2.3B) to the moment of incipient stage of the fault (Figure 2.3A) on the other side of the ridge axis. I use residual force defined as a sum of constant boundary force and internal force (Equation 2.3).

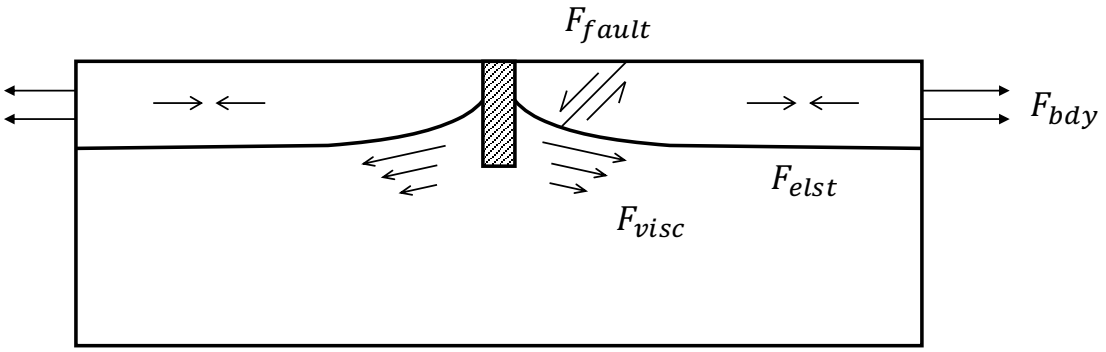

Fig. 2.4: Schematic illustration of the internal forces and boundary forces applying to the model.

$$F_{res} = F_{int} + F_{bdy} \tag{2.3}$$

$$= F_{fault} + F_{elst} + F_{visc} + F_{bdy} \tag{2.4}$$

Chapter 3

Results

Plate velocity varies with fault evolution

Fault development at a ridge affects plate velocity. In kinematic models, normal fault migrates away from the axis at a rate $U = 2v(M - 0.5)$, where v is a constant plate driving velocity (Figure 3.1) (Buck et al., 2005). Similarly, in the cases of force driven model, interaction between dynamic driving velocity from boundary force and opposite direction velocity from normal fault controls the plate speed in force. The plate containing active fault is slower than another plate.

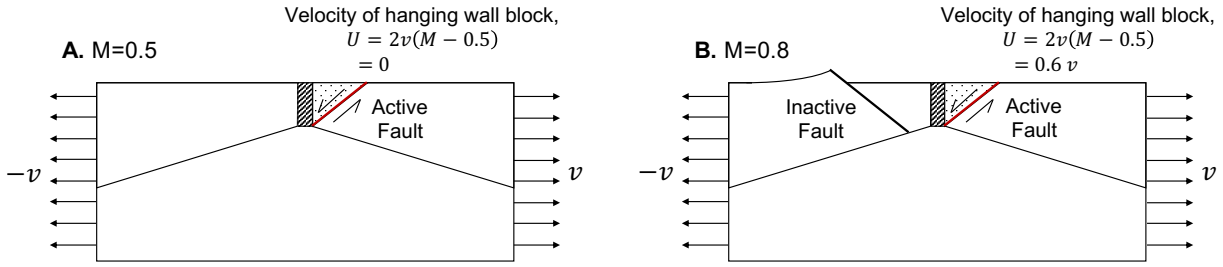

Fig. 3.1: **A.** Schematic model showing velocity of plate including active fault at mid-ocean ridges driven by velocity when M = 0.5. **B.** Same as **A** but for M = 0.8.

M = 0.5

When $M = 0.5$, half portion of plate spreading is accommodated by faulting and the master detachment fault forms because the fault ceases to migrate. In my model, the expected faulting mode lasts until 650 Kyrs.

Unlike velocity-driven model, force-driven model shows significant velocity changes over time. The detachment fault forms at *yrs on left side of the spreading axis. After *yrs, the left plate moves slowly.

M = 0.8

When $M = 0.8$, fault migrates toward off-axis. The fault eventually becomes inactive and is replaced by new and near-axis fault.

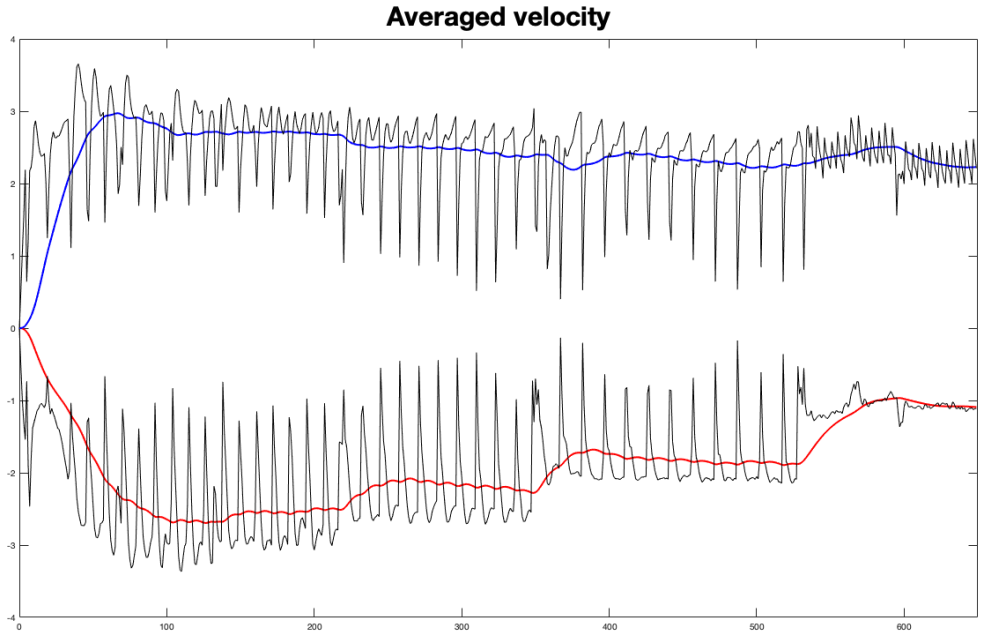

Fig. 3.2: Plate velocity obtained from M = 0.5 model results. Abnormal peaks from remeshing effects are filtered out.

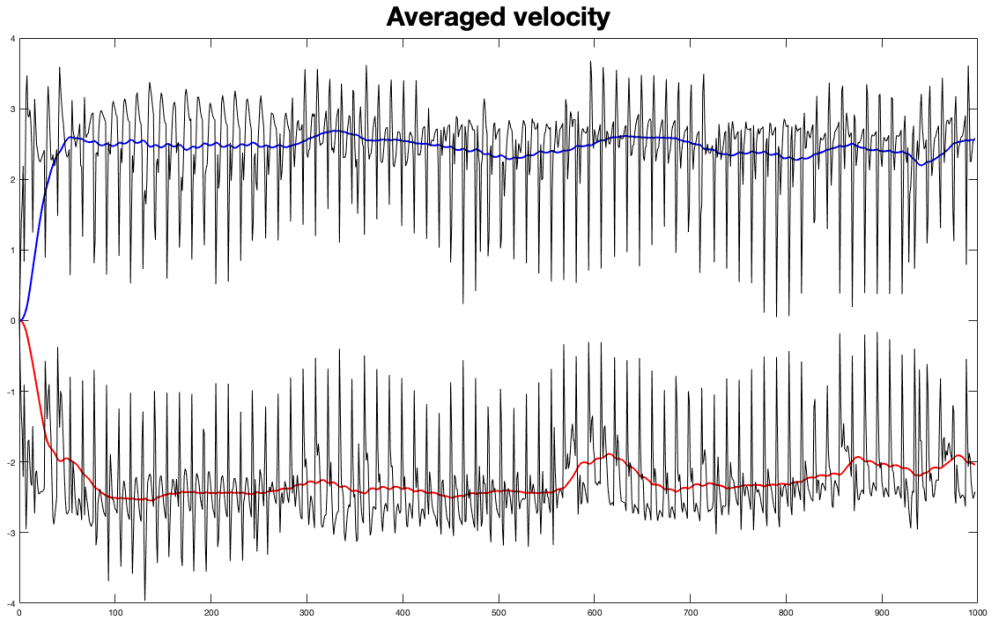

Fig. 3.3: Plate velocity obtained from M = 0.8 model results. Abnormal peaks from remeshing effects are filtered out.

Thermal state

Long term and large magnitude variation which cannot be explained by fault evolution may be caused by changes of the plate thermal state. By varying heat injection rate of the model, different behaviors of long term and large magnitude plate speed variation are observed.

Chapter 4

Discussion

Chapter 5

Conclusion

REFERENCES

Behn, M. D. & Ito, G. (2008), 'Magmatic and tectonic extension at mid-ocean ridges: 1. Controls on fault characteristics', *Geochem. Geophys. Geosyst.* **9**.

Brune, S., Williams, S. E., Butterworth, N. P. & Müller, R. D. (2016), 'Abrupt plate accelerations shape rifted continental margins', *Nature* **536**(7615), 201–204.
URL: *http://dx.doi.org/10.1038/nature18319*

Buck, W. R., Lavier, L. L. & Poliakov, A. N. (2005), 'Modes of faulting at mid-ocean ridges', *Nature* pp. 719–723.

Buck, W. R. & Poliakov, A. N. (1998), 'Abyssal hills formed by stretching oceanic lithosphere', *Nature* **392**(march), 272–275.

Cann, J. R. (1968), 'Geological Processes at Mid-Ocean Ridge Crests', *Geophysical Journal of the Royal Astronomical Society* **15**(3), 331–341.

Castelino, J. A., Eagles, G. & Jokat, W. (2016), 'Anomalous bathymetry and palaeobathymetric models of the Mozambique Basin and Riiser Larsen Sea', *Earth and Planetary Science Letters* **455**, 25–37.
URL: *http://dx.doi.org/10.1016/j.epsl.2016.09.018*

Chen, Y. J. (1992), 'Oceanic crustal thickness versus spreading rate', *Geophysical Research Letters* **19**(8), 753–756.
URL: *https://agupubs.onlinelibrary.wiley.com/doi/abs/10.1029/92GL00161*

Chen, Y. & Morgan, W. J. (1990), 'A nonlinear rheology model for mid-ocean ridge axis topography', *Journal of Geophysical Research: Solid Earth* **95**(B11), 17583–17604.
URL: *https://agupubs.onlinelibrary.wiley.com/doi/abs/10.1029/JB095iB11p17583*

Cundall, P. A. (1982), 'Adaptive Density-Scaling for Time-Explicit Calculations', *Proceedings of the 4th International Conference on Numerical Methods in Geomechanics (Edmonton, 1982)*

1, 23–26.

URL: *http://ci.nii.ac.jp/naid/80001531101/en/*

Fedotova, A., Reece, B., Goff, J., Christeson, G., Estep, J., Carlson, R., Skipwith, J. & Bonnette, G. (2017), 'Variation in Abyssal Hill Geomorphology in the South Atlantic Ocean', *T219-430 presented at Geological Society of America 129th Annual Meeting, Seattle, WA, 22-25 Oct.* .

Flament, N., Gurnis, M., Williams, S., Seton, M., Skogseid, J., Heine, C. & Dietmar Müller, R. (2014), 'Topographic asymmetry of the South Atlantic from global models of mantle flow and lithospheric stretching', *Earth and Planetary Science Letters* **387**, 107–119.

URL: *http://dx.doi.org/10.1016/j.epsl.2013.11.017*

Hess, H. H. (1964), 'Seismic Anisotropy of the Uppermost Mantle under Oceans', *Nature* **203**, 629.

URL: *http://dx.doi.org/10.1038/203629a0 http://10.0.4.14/203629a0*

Kirby, S. H. & Kronenberg, A. K. (1987), 'Rheology of the lithosphere: Selected topics', *Reviews of Geophysics* **25**(6), 1219–1244.

Lavier, L. L. & Buck, W. R. (2002), 'Half graben versus large-offset low-angle normal fault : Importance of keeping cool during normal faulting', *Journal of Geophysical Research* **107**, 1–16.

Martinez, F., Taylor, B., Baker, E. T., Resing, J. A. & Walker, S. L. (2006), 'Opposing trends in crustal thickness and spreading rate along the back-arc Eastern Lau Spreading Center: Implications for controls on ridge morphology, faulting, and hydrothermal activity', *Earth and Planetary Science Letters* **245**(3-4), 655–672.

Müller, R. D., Roest, W. R. & Royer, J.-Y. (1998), 'Asymmetic seafloor spreading expresses ridge- plume interactions', **396**(December), 455–459.

Müller, R. D., Sdrolias, M., Gaina, C. & Roest, W. R. (2008), 'Age, spreading rates, and spreading asymmetry of the world's ocean crust', *Geochemistry, Geophysics, Geosystems* **9**(4), 1–19.

Peltier, W. R. (1989), *Mantle Convection: Plate Tectonics and Global Dynamics*, Gordon and Breach Science Publishers.

Poliakov, A. N. B. & Buck, W. R. (1998), *Mechanics of Stretching Elastic-Plastic-Viscous Layers: Applications to Slow-Spreading Mid-Ocean Ridges*, American Geophysical Union (AGU), pp. 305–323.
URL: *https://agupubs.onlinelibrary.wiley.com/doi/abs/10.1029/GM106p0305*

Poliakov, A. N. B., Cundall, P. A., Podladchikov, Y. Y. & Lyakhovsky, V. A. (1993), *An Explicit Inertial Method for the Simulation of Viscoelastic Flow: An Evaluation of Elastic Effects on Diapiric Flow in Two- and Three- Layers Models*, Springer Netherlands, Dordrecht, pp. 175–195.
URL: *https://doi.org/10.1007/978-94-015-8206-3_12*

Tucholke, B. E., Behn, M. D., Buck, W. R., Lin, J., Tucholke, B. E., Hole, W., Hole, W. & Behn, M. D. (2008), 'Role of melt supply in oceanic detachment faulting and formation of megamullions', *Geology* **36**, 455–458.